Molecular Structural Dynamics in Water-Ethanol Mixtures: Spectroscopy with Polarized Neutrons Simultaneously Accessing Collective and Self-Diffusion – Supplementary Material –

Riccardo Morbidini[1,2], Robert M. Edkins[3], Mark Devonport[4], Gøran Nilsen[4], Tilo Seydel[1,*], and Katharina Edkins[2,*]

[1]*Institut Max von Laue - Paul Langevin, 71 Avenue des Martyrs, F-38042 Grenoble, France*
[2]*Division of Pharmacy and Optometry, University of Manchester, Oxford Road, Manchester M13 9PT, United Kingdom*
[3]*WestCHEM Department of Pure and Applied Chemistry, University of Strathclyde, 295 Cathedral Street, Glasgow G1 1XL, United Kingdom*
[4]*ISIS Neutron and Muon Source, Rutherford Appleton Laboratory, Didcot, OX11 0QX, United Kingdom*
[*]*Corresponding authors: seydel@ill.eu, katharina.edkins@manchester.ac.uk*

S1 Polarization analysis

In a quasi elastic scattering experiment, both collective and self motions contribute to the broadening of the elastic peak (figure S1), and the double differential scattering cross section, *i.e.* the probability that a neutron is scattered by a nucleus into a solid angle element $\partial\Omega$ and with a change in energy $\partial\hbar\omega$, thus reads as linear combination of the coherent $S^{\mathrm{coh}}(q,\omega)$ and incoherent $S^{\mathrm{inc}}(q,\omega)$ dynamic structure factors

$$\frac{\partial^2\sigma}{\partial\Omega\partial\hbar\omega} \propto \sum_{\alpha,\beta} \bar{b_\alpha}\bar{b_\beta} S^{\mathrm{coh}}_{\alpha\beta}(q,\omega) + \sum_{\alpha} \Delta\bar{b}^2_\alpha S^{\mathrm{inc}}_{\alpha}(q,\omega) \tag{1}$$

where the sums run over the atomic species α,β (H, D, O and C for water-ethanol mixtures) weighted by their scattering lengths $b_{\alpha,\beta}$. $S^{\mathrm{coh}}(q,\omega)$ and $S^{\mathrm{inc}}(q,\omega)$ are related via time and real space Fourier transform to the Van Hove correlation functions $G_{\alpha\beta}(r,t)$ and $G^{\mathrm{self}}_{\alpha}(r,t)$ describing the correlations between the position of distinct nuclei at different times and of the same nucleus at different times, respectively. For the majority of studied systems $\frac{\partial^2\sigma}{\partial\Omega\partial\hbar\omega} \simeq S^{\mathrm{inc}}(q,\omega)$ due to the ubiquitous presence of hydrogen atoms whose scattering is predominantly incoherent. However, this approximation shows limits for poorly incoherent scattering samples or for those systems in which the solvent contribute is masked by deuteration. In this cases both coherent and incoherent terms coexist making data interpretation more complex. The only way to decouple the two contributions from eqn.(1) is by polarization analysis (PA), a method that relies on the principles that the neutron scattering probability is not only isotope but also spin-dependent and that for incoherent scattering the neutron spin has a 66% probability to flip while for coherent scattering no spin flip happens. In an unpolarized experiment the incident neutron beam has 50% of spin up $|\uparrow\rangle$ and 50% of spin down $|\downarrow\rangle$ neutrons while with PA a supermirror polarizer is implemented to transmit the $|\downarrow\rangle$ state of the neutron beam. In order to exploit the link between spin-flip $|\downarrow\rangle \rightarrow |\uparrow\rangle$/non-spin-flip $|\downarrow\rangle \rightarrow |\downarrow\rangle$ and incoherent $S^{\mathrm{inc}}(q,\omega)$/coherent $S^{\mathrm{coh}}(q,\omega)$ dynamic structure factors, spin are reversed using a precession coil flipper and the spin polarization of the scattered neutron beam is analyzed.[1,2] On LET this last step is made with a ^{3}He spin filter with a typical initial polarization of 63% and lifetime of 48 hours. The cell was replaced every $\sim$ 24 hours. The polarization corrections were performed using the correction scheme described in Ref.[3]. The combined flipper and polarizer efficiencies for the three incident energies E_i = 3.84, 1.81, 1.05 meV were 90%, 91%, and 91%, respectively.

The result of this process are two distinct dynamic structure factors related to spin-flip $S_{|\downarrow\rangle\rightarrow|\uparrow\rangle}(q,\omega)$ and non-spin-flip $S_{|\downarrow\rangle\rightarrow|\downarrow\rangle}(q,\omega)$ events which are then combined to obtain the separation between $S_{\mathrm{inc}}(q,\omega)$ and $S_{\mathrm{coh}}(q,\omega)$ as follows:

$$\begin{cases} S_{|\downarrow\rangle\rightarrow|\uparrow\rangle}(q,\omega) = S_{\mathrm{coh}}(q,\omega) + \frac{1}{3}S_{\mathrm{inc}}(q,\omega) \\ S_{|\downarrow\rangle\rightarrow|\downarrow\rangle}(q,\omega) = \frac{2}{3}S_{\mathrm{inc}}(q,\omega) \end{cases} \quad \begin{cases} S_{\mathrm{coh}}(q,\omega) = S_{|\downarrow\rangle\rightarrow|\downarrow\rangle}(q,\omega) - \frac{1}{2}S_{|\downarrow\rangle\rightarrow|\uparrow\rangle}(q,\omega) \\ S_{\mathrm{inc}}(q,\omega) = \frac{3}{2}S_{|\downarrow\rangle\rightarrow|\uparrow\rangle}(q,\omega) \end{cases} \tag{2}$$

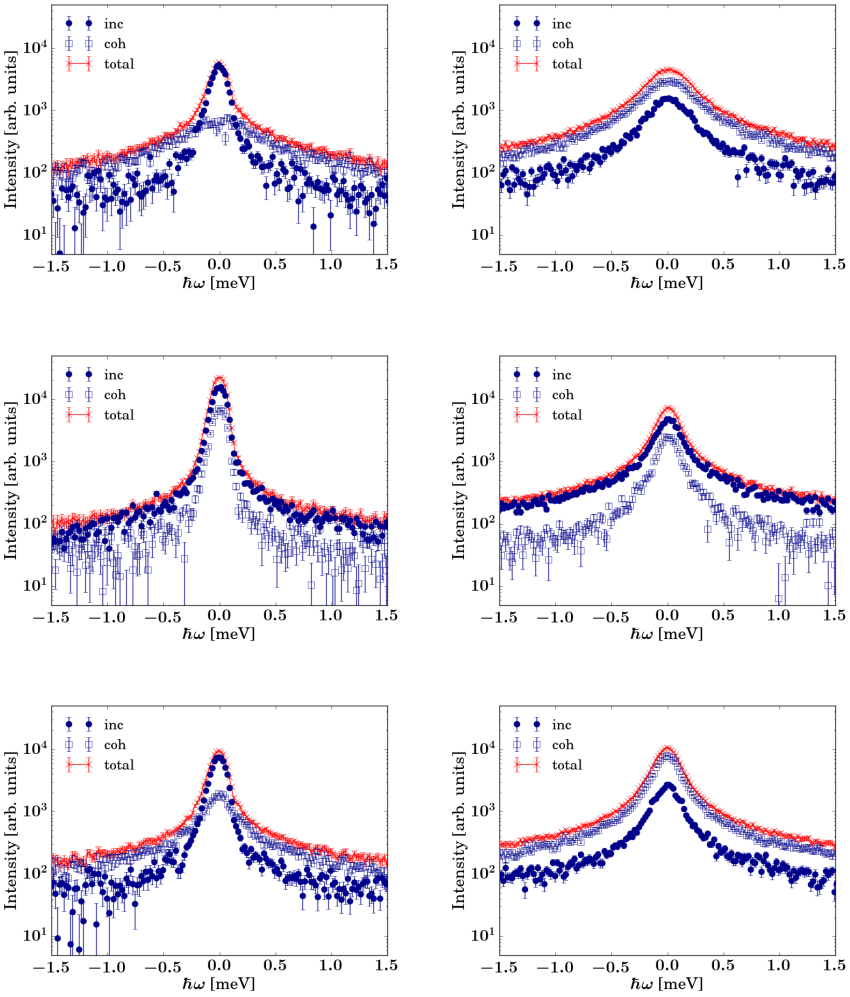

Fig. S1: Comparison of the coherent (empty squares), incoherent (dark full circles) and total (red crosses) scattering functions measured on LET at q = 1.0 Å^{-1} (left column) and q = 1.9 Å^{-1} (right column). In the case of pure D_2O (top row) the coherent spectrum becomes dominant at higher q, corresponding to $S(q)$. At lower q, the incoherent spectrum is dominant and, thus, polarization analysis becomes crucial to obtain collective-like dynamic information. When mixed with C_2H_5OD (0.12 ethanol mole fraction, middle row) there is no q value where the coherent signal is dominant so polarization is even more crucial to account for collective motion even at the intramolecular scale. The fully deuterated mixture D_2O/C_2D_5OD (0.12 ethanol mole fraction, bottom row), on the other hand, shows a similar behaviour to that of pure D_2O.

S2 Instrument resolution

Instrument resolution has been accounted for by fitting the vanadium incoherent spectrum with a sum of up to five Gaussian functions (depending on q and incident energy), due to the asymmetric shape of the instrument response (Fig. S2).

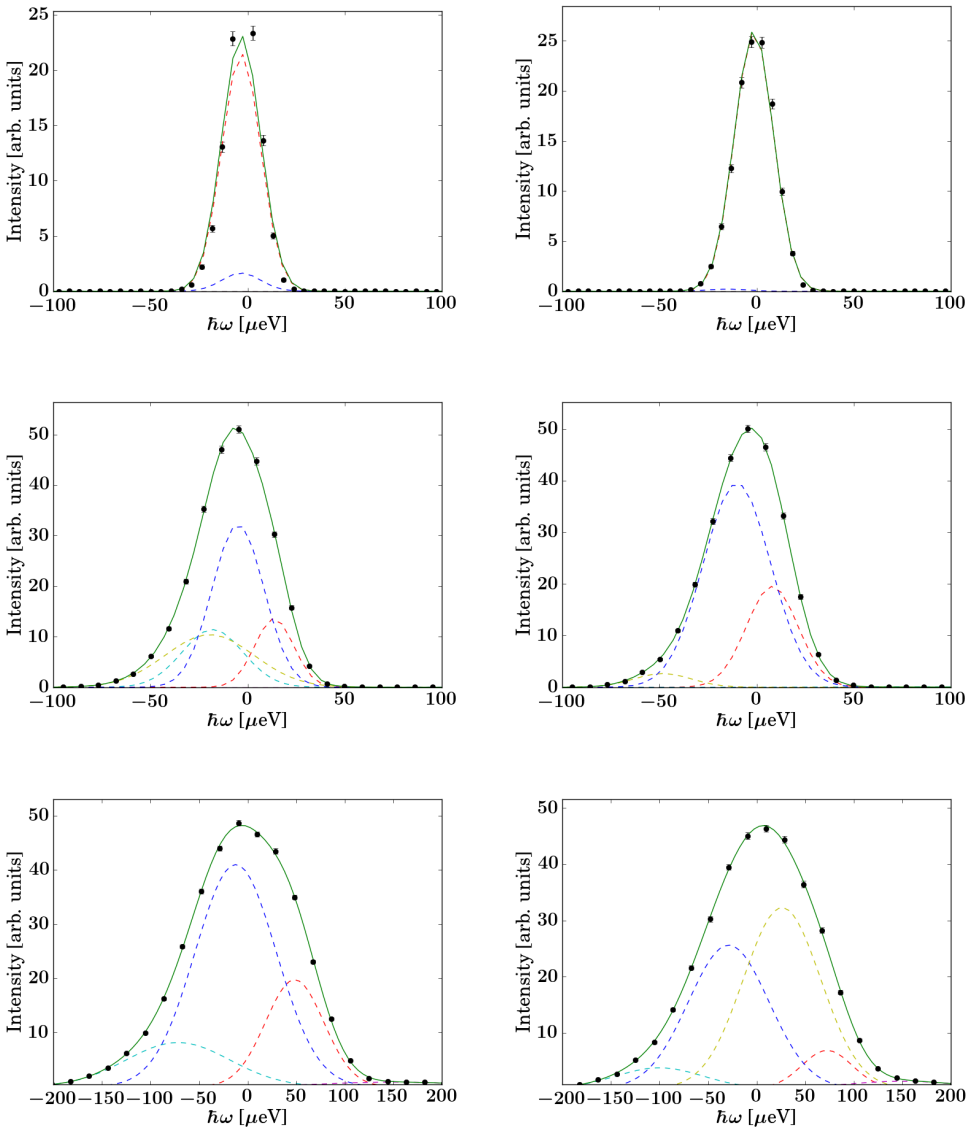

Fig. S2: Energy resolution data of LET (symbols), measured on Vanadium foil at T = 285K, and fits of a sum (solid lines) of up to 5 Gaussian functions (dashed lines), at q = 0.7 Å^{-1} (left column) and q = 1.1 Å^{-1} (right column). The three different incident energies $E_i = 1.05$ meV (first row), 1.81 meV (second row) and 3.84 meV (third row) provide three distinctly different widths which each weakly depend on q.

S3 Self-diffusion in the partially deuterated mixture

Example spectra

To favour convergence of the fit to physically meaningful values, the second Lorentzian has been constrained to be broader than the first Lorentzian, in agreement with a convolution of these two motions, as done in previous work.[4] This constraint prevented cross-talking (i.e. inversion) between the two Lorentzian functions during the iterative least squares minimization. The essential fit parameters and goodness-of-fit χ^2 are summarized in the figures S4 and S5 for different mixing ratios. Other models have been tested as well, including a Dirac contribution to account for immobile fractions and un-subtracted empty cell signal, but the finally chosen model presented was the most aligned with the experimental data.

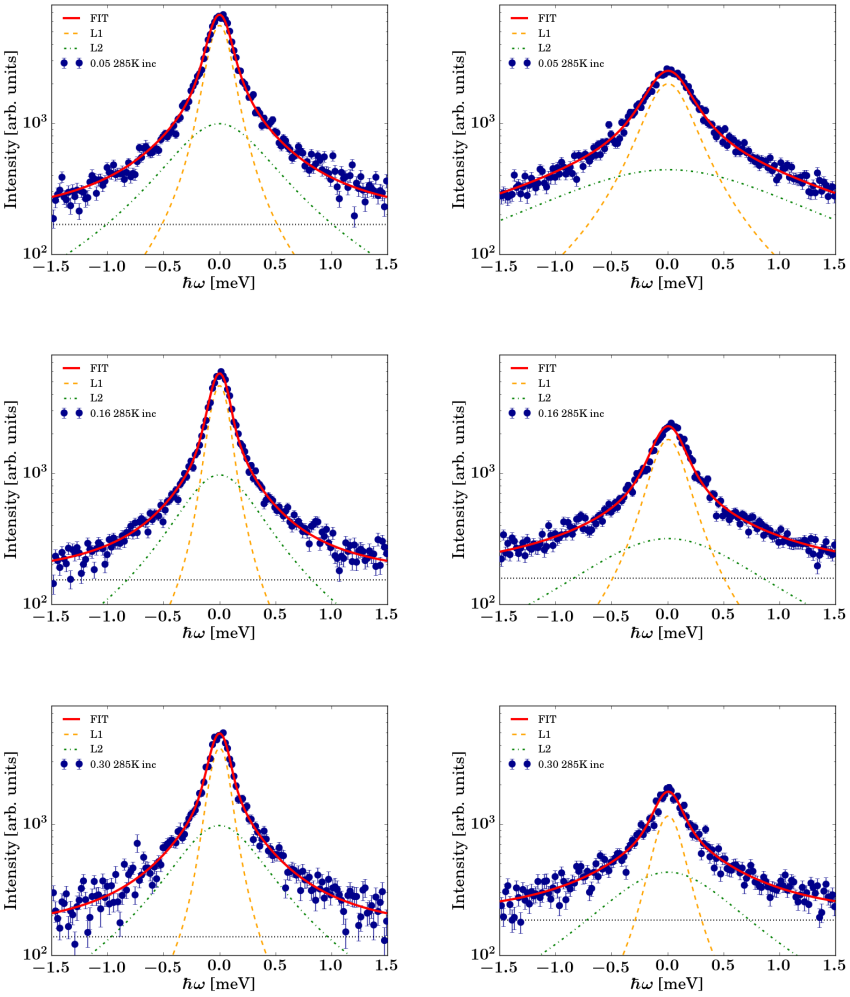

Fig. S3: Example incoherent scattering function at q=1.3 Å^{-1} (left column) and q=2.1 Å^{-1} (right column) recorded on LET at E_i=3.84 meV at T=285K. Fit (red solid line) according to eqn. 1 of the main text consisting of a sum of two Lorentzians (dashed and dash-dotted line) and an almost negligible flat apparent background (dotted line). Top row: 0.05 ethanol mole fraction, middle row: 0.16 ethanol mole fraction, bottom row, 0.3 ethanol mole fraction.

Fit parameters

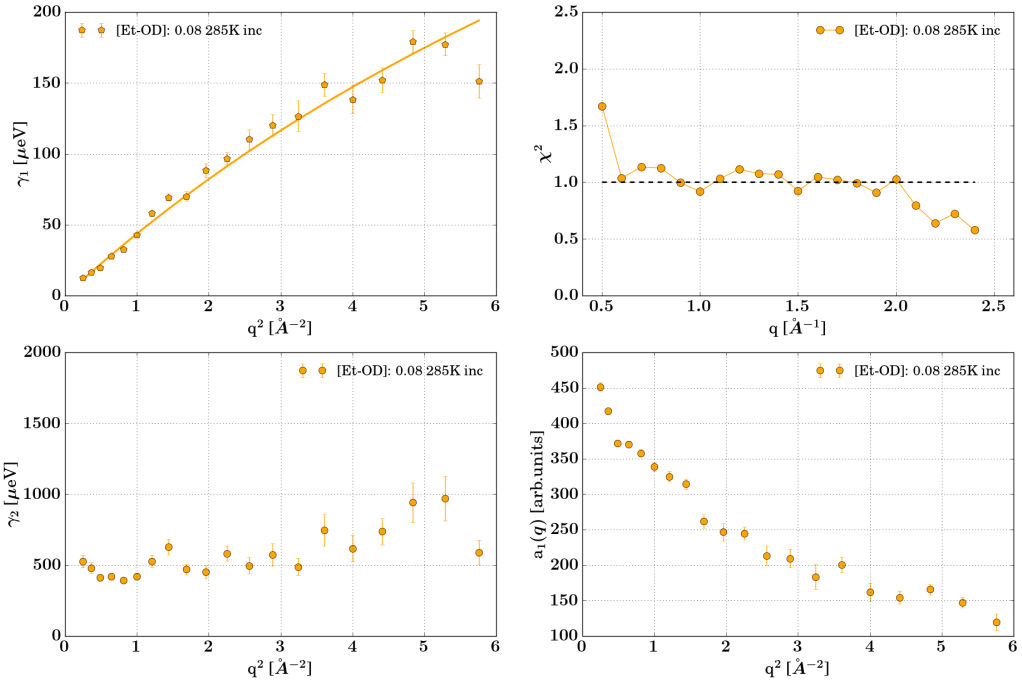

Fig. S4: Plot of the fit parameters according to eqn. 1 of the main text for D_2O/C_2H_5OD at 0.08 ethanol mole fraction, at T=285K and E_i=3.84meV. Top left: Lorentzian width $\gamma_1(q)$ associated with the center of mass translation of the molecule. The solid line stands for the fit of the jump diffusion model. Bottom left: Lorentzian width of the second faster process $\gamma_2(q)$ that can be attributed to localized motions with no marked q-dependence. Top right: reduced χ^2 for the fit. Bottom right: Intensity of the first Lorentzian $a_1(q)$.

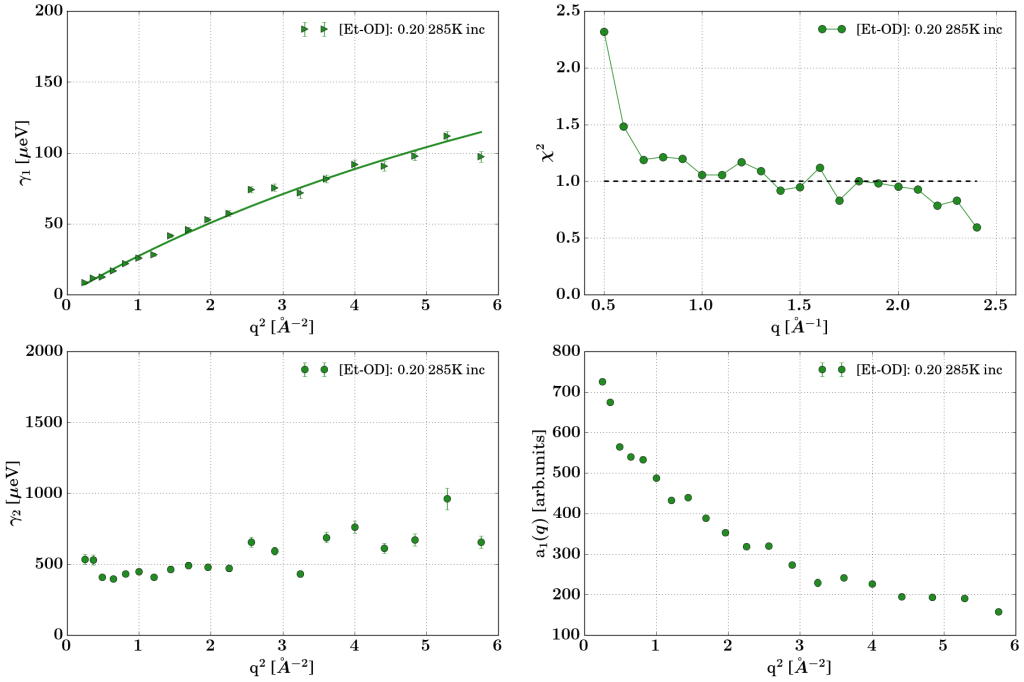

Fig. S5: Plot of the fit parameters according to eqn. 1 of the main text for D_2O/C_2H_5OD at 0.2 ethanol mole fraction, at T=285K and E_i=3.84meV. Top left: Lorentzian width $\gamma_1(q)$ associated with the center of mass translation of the molecule. The solid line stands for the fit of the jump diffusion model. Bottom left: Lorentzian width of the second faster process $\gamma_2(q)$ that can be attributed to localized motions with no marked q-dependence. Top right: reduced χ^2 for the fit. Bottom right: Intensity of the first Lorentzian $a_1(q)$.

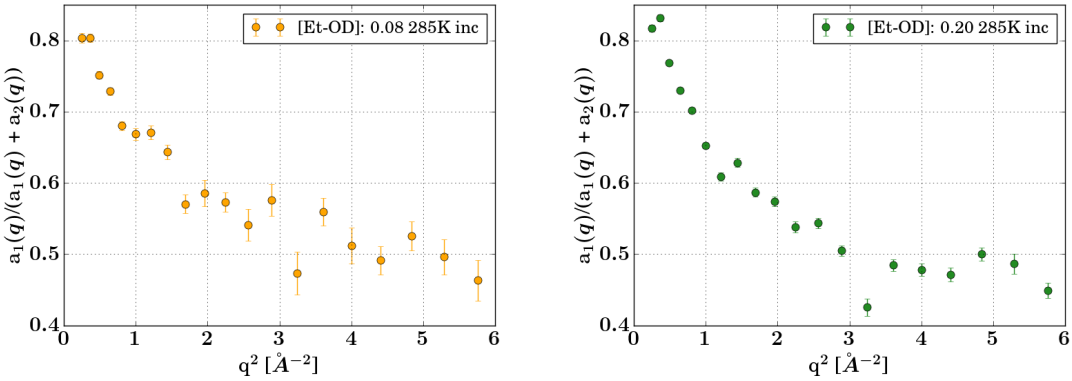

Fig. S6: Fractional intensity of the first Lorentzian $a_1(q)/(a_1(q)+a_2(q))$ for 0.08 (left) and 0.2 (right) ethanol mole fraction.

S4 Collective diffusion in the partially deuterated mixture

We also tested the same approach employed for the incoherent spectra on coherent spectra, i.e., imposing a sum of two Lorentzians convoluted with the spectrometer resolution (see Figure S7-S8 below). However, the lack of a theoretical model to interpret the quasi-elastic signal of the coherent part of the spectrum prevents us from interpreting the underlying collective dynamics.
One heuristic approach is to relate collective to single particle motion via renormalization by the static structure factor $S(q)$ as proposed by Sköld[5]:

$$\frac{S_{coh}(q,\omega)}{S(q)} \approx S_{inc}\left(\frac{q}{\sqrt{S(q)}},\omega\right) \tag{3}$$

We did not follow this approach for two main reasons:
(1) It fails to predict the correct q-dependence of $S(q,\omega)$ at q lower than the peak of the structure factor[6]. This would affect our observations which are more pronounced in the mesoscale.
(2) The interpretation of the resulting apparent collective diffusion function $D_c(q)$ would be subject to the same lack of theory.
In contrast, the susceptibility picture provides these advantages:
- In this representation, well separated peaks allow to distinguish distinct processes.
- The results can be directly compared with dielectric spectroscopy.
- Due to the novelty of our data, we benefit from relying on an established approach for data analysis, permitting to compare with the work on pure D_2O.
- The effect of the instrument resolution at ambient temperature does not pose a substantial problem since the dynamics is sufficiently fast. It would be a limit for systems with slower dynamics, such as in the supercooled regime.

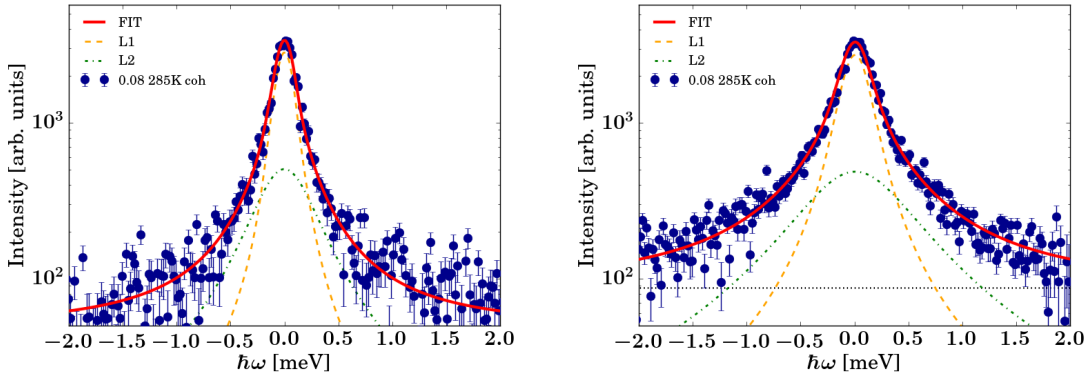

Fig. S7: Example coherent scattering function at q=1.3 Å^{-1} (left column) and q=2.1 Å^{-1} (right column) recorded on LET at E_i=3.84 meV, T=285K and 0.08 ethanol mole fraction. Fit (red solid line) according to eqn. 1 of the main text consisting of a sum of two Lorentzians (dashed and dash-dotted line) and an almost negligible flat apparent background (dotted line).

Coherent susceptibility

The conversion to susceptibility $\chi''_{\rm coh}(q,\omega)$ and the model used to fit $\chi''_{\rm coh}(q,\omega)$ is inspired by previous neutron work on polarized neutrons[7]

$$\chi(q,\nu) \simeq \frac{1}{1+i\omega\tau} \tag{4}$$

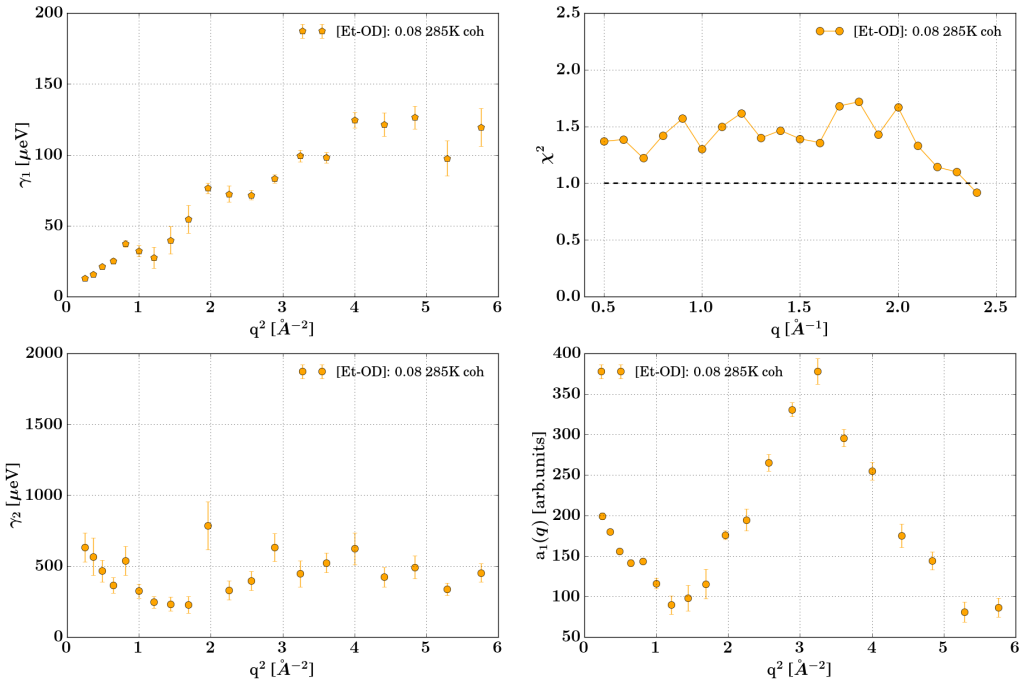

Fig. S8: Plot of the fit parameters according to eqn. 1 of the main text for D_2O/C_2H_5OD at 0.08 ethanol mole fraction, at T=285K and E_i=3.84meV. Top left: Lorentzian width $\gamma_1(q)$. Bottom left: Lorentzian width of the second faster process $\gamma_2(q)$ that can be attributed to localized motions with no marked q-dependence. Top right: reduced χ^2 for the fit. Bottom right: Intensity of the first Lorentzian $a_1(q)$.

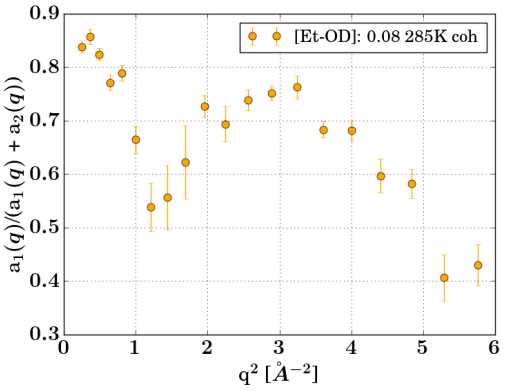

Fig. S9: Fractional intensity of the first Lorentzian $a_1(q)/(a_1(q) + a_2(q))$ for the experimental parameters as in the preceding figure S8.

with the imaginary part given by

$$\chi''(q,\nu) \simeq \frac{\omega\tau}{1+\omega^2\tau^2}. \tag{5}$$

The more general case of this symmetric and not stretched Lorentzian-like function is called Havriliak-Negami relaxation, where the asymmetry and broadness are accounted for, through the two terms α and β,

$$\chi(q,\nu) \simeq \frac{1}{(1+(i\omega\tau)^{\alpha})^{\beta}}. \tag{6}$$

For $\beta = 1$ the Havriliak-Negami reduces to the Cole-Cole equation,

$$\chi''(q,\nu) \simeq \frac{(\omega\tau)^{1-\alpha} cos(\alpha\pi/2)}{1+2(\omega\tau)^{1-\alpha}\sin(\alpha\pi/2)+(\omega\tau)^{2(1-\alpha)}}, \tag{7}$$

and for $\alpha = 1$ to the Cole-Davidson relaxation,

$$\chi''(q,\nu) \simeq (1+(\omega\tau)^2)^{-\beta/2}\sin(\beta\arctan(\omega\tau)). \tag{8}$$

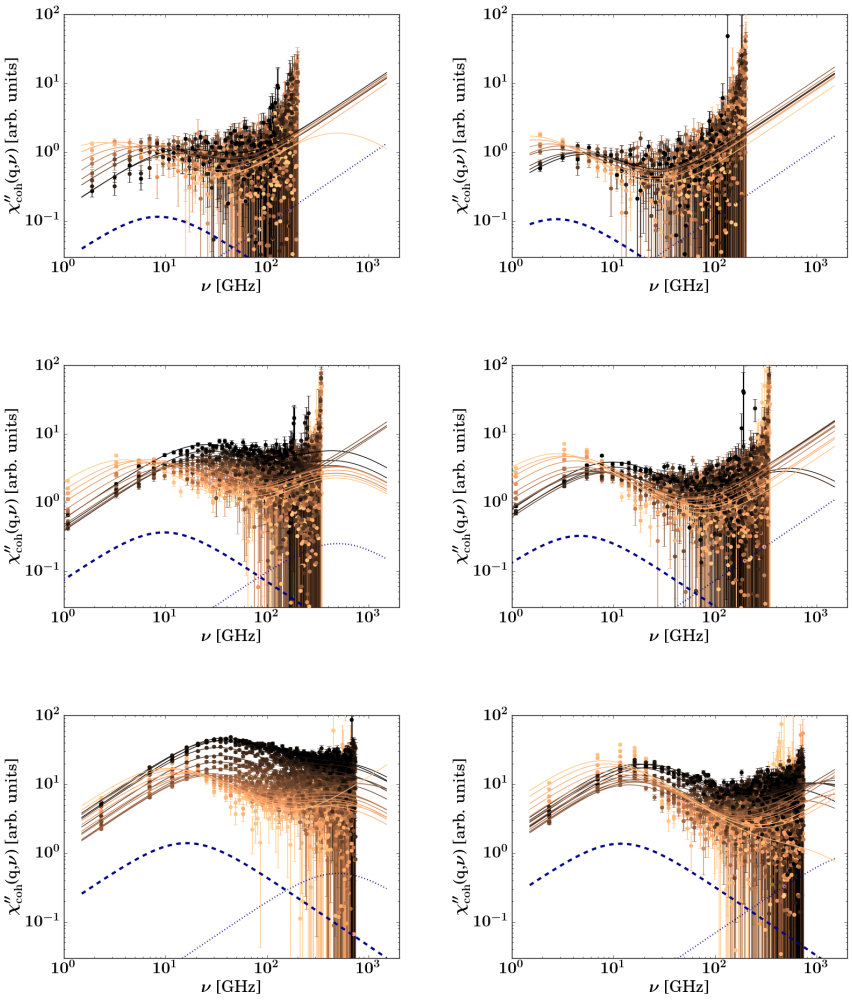

Fig. S10: Imaginary part of the dynamical susceptibility for the coherent spectrum of D_2O/C_2H_5OD at 0.05 ethanol mole fraction (left column) and at 0.20 ethanol mole fraction (right column). The solid lines stand for the fit according to eqn. 3 of the main text with blue dashed and dotted lines depicting the main and the second Debye process (scaled by a factor 0.6 for visibility) respectively. Top row: E_i=1.05 meV in the range (orange) $0.4\,\text{Å}^{-1} \leq q \leq 1.1\,\text{Å}^{-1}$ (black); middle row: E_i=1.81 meV in the range (orange) $0.4\,\text{Å}^{-1} \leq q \leq 1.5\,\text{Å}^{-1}$ (black); bottom row: E_i=3.84 meV in the range (orange) $0.4\,\text{Å}^{-1} \leq q \leq 1.9\,\text{Å}^{-1}$ (black).

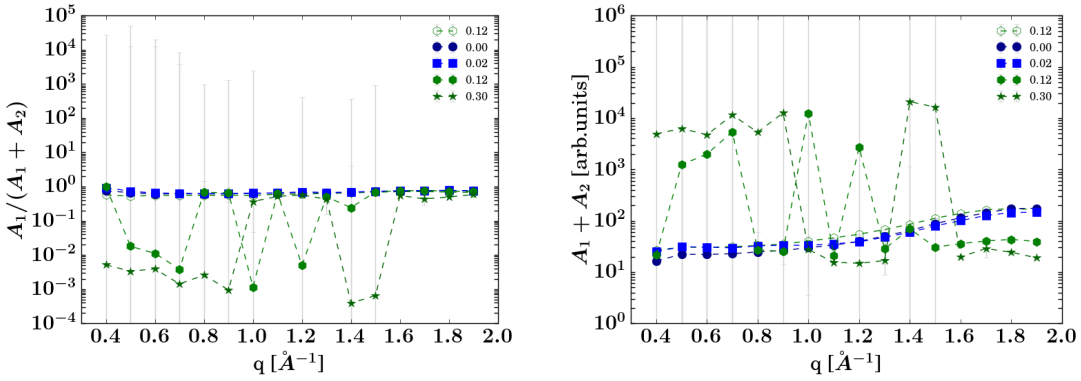

Fig. S11: Left: Fractional amplitude $A_1(q)/(A_1(q)+A_2(q))$ of the main relaxation process of $\chi''(q,\nu)$ as a function of ethanol mole fraction at T=285K and for E_i=3.84 meV. Right: Total amplitude $A_1(q)+A_2(q)$. (Cf. eqn. 3 of the main text.) Due to the poorer statistics when approaching the THz regime the parameters of the second process A_2 and τ_2, representing the vibrational relaxation, display broad confidence bounds (grey), especially at low q.

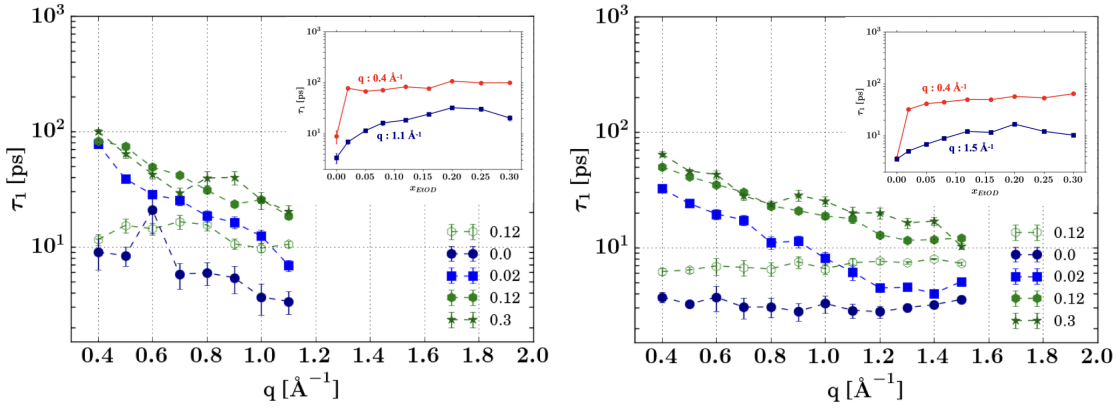

Fig. S12: Relaxation times $\tau_1(q)$ (symbols) of the main relaxation process of $\chi''_{\rm coh}(q,\nu)$ as a function of q (main parts, ethanol mole fractions specified in the legends) and as a function of ethanol mole fraction for two distinct q values (insets, q values specified next to the lines), respectively, at T=285K and for E_i=1.05meV (left) and E_i=1.81meV (right). The lines are guides to the eye.

Incoherent susceptibility

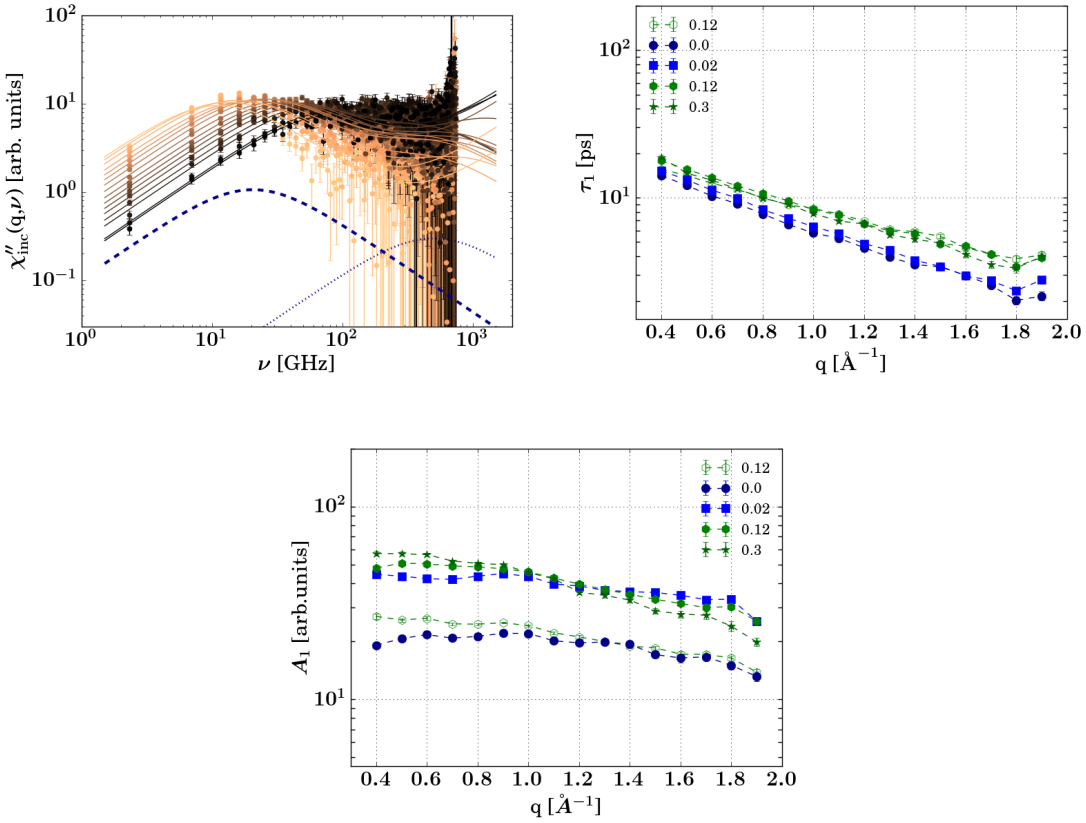

Fig. S13: Top left: Imaginary part of the dynamical susceptibility for the incoherent spectrum of D_2O recorded at T=285K with E_i=3.84meV in the range $0.4\,\text{Å}^{-1} \leq q \leq 1.9\,\text{Å}^{-1}$. Top right: Relaxation times $\tau_1(q)$ and amplitude $A_1(q)$ (bottom) of the main relaxation process of $\chi''_{\text{inc}}(q,\nu)$ as a function of ethanol mole fraction at T=285K and for E_i=3.84meV. Values obtained from the peak position of $\nu_i^{\max} = (2\pi\tau_1)^{-1}$.

S5 Apparent static structure factors

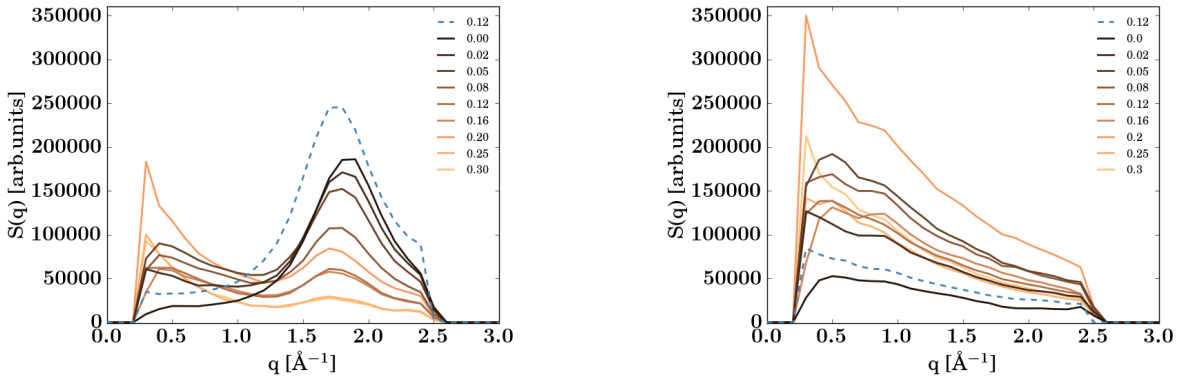

Fig. S14: Apparent static structure factor depending on the ethanol-D_2O mixing ratio (cf. legend) obtained by integrating the coherent part (left) and incoherent part (right) of the LET dynamic scattering function $S(q,\omega)$ in the range $-260\mu eV \leq \hbar\omega \leq 260\mu eV$, which corresponds to approximately twice the spectrometer resolution line width at this incident energy ($E_i = 3.84$ meV, cf. figure S2). The dashed blue lines report the per-deuterated spectrum measured on the mixture of D_2O and C_2D_5OD. The intensities of $S(q)$ are proportional to the measured intensities normalized to the incident beam intensities. The left and right plots are drawn on the same scale to render the coherent and incoherent intensities comparable across the plots. The change in absolute intensity depending on the mixing ratio mainly arises from the changing total coherent cross section. In the coherent part (left) we identify a local maximum which might be associated with the pre-peak near $0.4\,\text{Å}^{-1}$ and the liquid structure peak near $1.6\,\text{Å}^{-1}$. We note that these observations can depend on dynamical and instrumental effects. Nevertheless, a corresponding observation, i.e., the presence of a pre-peak in the partially deuterated mixture and its absence in the per-deuterated mixture has been reported for methanol solutions based on CD_3OD and CH_3OD, respectively (cf. main article for a discussion).

S6 Cross sections

Due to the high degree of polarization and the long measurement time the scattering signal, both coherent and incoherent, is sufficient for all mixing ratios (see Fig. S1). Indeed, due to selective deuteration and polarization analysis we can differently weigh different species within the different samples. In this regard, in Fig.S15 we report the total scattering cross section Σ^i for the incoherent, coherent and sum obtained by

$$\Sigma^i = n_{D_2O}\sigma^i_{D_2O} + n_{EtOD}\sigma^i_{EtOD} = \frac{N_A\rho_{D_2O}(1-x_{EtOD})}{M_{D_2O}}\sigma^i_{D_2O} + \frac{N_A\rho_{EtOD}x_{EtOD}}{M_{EtOD}}\sigma^i_{EtOD} \tag{9}$$

with the number density n expressed in term of the Avogadro number N_A, the density ρ, molecular weight M, ethanol mole fraction x_{EtOD}, and $i \in \{\text{inc}, \text{coh}, \text{tot}\}$. As shown in this figure, the incoherent cross section increases with increasing ethanol ratio, and it exceeds the coherent one near 8% ethanol contents. Between the extremes of the mixing ratios (100% water and 100 $\%$ Ethanol, respectively) the incoherent signal rapidly shifts from being due to D_2O to be dominated by ethanol.

Data accessibility

The neutron data are permanently curated by the ISIS facility and accessible via `https://doi.org/10.5286/ISIS.E.RB1920548` and `https://doi.org/10.5286/ISIS.E.RB2210240`.

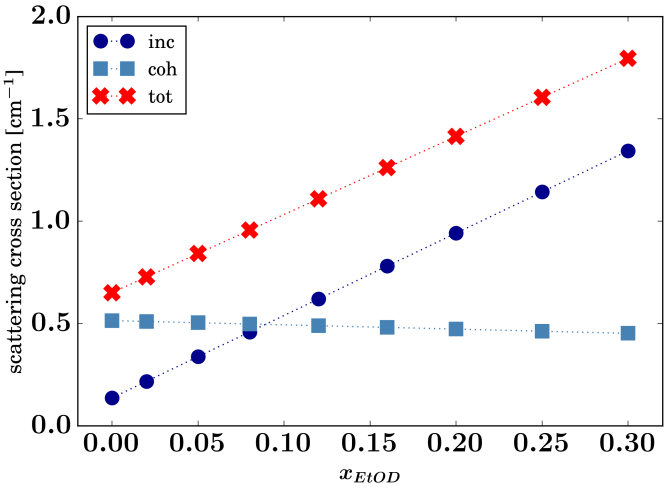

Fig. S15: Scattering cross sections as a function of ethanol mole fraction, calculated from eq.9 with NIST values for isotopes cross sections (b=$10^{-24}\mathrm{cm}^2$).

References

[1] G J Nilsen, J Košata, M Devonport, P Galsworthy, R I Bewley, D J Voneshen, R Dalgliesh, and J R Stewart. Polarisation analysis on the LET time-of-flight spectrometer. *J. Physics: Conference Series*, 862(1):012019, jun 2017.

[2] J. Košata, G.J. Nilsen, M. Devonport, R.I. Bewley, D.J. Voneshen, P.J. Galsworthy, D. Raspino, and J.R. Stewart. Polarized primary spectrometer on the let instrument at isis. *Physica B: Condensed Matter*, 551:476–479, 2018. The 11th International Conference on Neutron Scattering (ICNS 2017).

[3] G Cassella, J R Stewart, G M Paternò, V García Sakai, M Devonport, P J Galsworthy, R I Bewley, D J Voneshen, D Raspino, and G J Nilsen. Polarization analysis on the let cold neutron spectrometer using a 3he spin-filter: First results. *J. Physics: Conference Series*, 1316(1):012007, oct 2019.

[4] Johan Qvist, Helmut Schober, and Bertil Halle. Structural dynamics of supercooled water from quasielastic neutron scattering and molecular simulations. *J. Chem. Phys.*, 134(14):144508, 2011.

[5] Kurt Sköld. Small energy transfer scattering of cold neutrons from liquid argon. *Phys. Rev. Lett.*, 19(18):1023, 1967.

[6] VN Novikov, Kenneth S Schweizer, and Alexei P Sokolov. Coherent neutron scattering and collective dynamics on mesoscale. *J. Chem. Phys.*, 138(16):164508, 2013.

[7] Arantxa Arbe, Gøran J Nilsen, J Ross Stewart, Fernando Alvarez, Victoria García Sakai, and Juan Colmenero. Coherent structural relaxation of water from meso- to intermolecular scales measured using neutron spectroscopy with polarization analysis. *Phys. Rev. Research*, 2(2):022015, 2020.